Quantum Master Equation Approach to Exciton Recurrence Motion in Ring-Shaped Aggregate Complexes Induced by Linear- and Circular-Polarized Laser Fields

ARTICLE *in* THE JOURNAL OF PHYSICAL CHEMISTRY C · FEBRUARY 2009

Impact Factor: 4.77 · DOI: 10.1021/jp8096555

7 AUTHORS, INCLUDING:

Kyohei Yoneda
Nara National College of Technology
42 PUBLICATIONS **599** CITATIONS
SEE PROFILE

Ryohei Kishi
Osaka University
110 PUBLICATIONS **1,955** CITATIONS
SEE PROFILE

Masayoshi Nakano
Osaka University
337 PUBLICATIONS **4,793** CITATIONS
SEE PROFILE

THE JOURNAL OF PHYSICAL CHEMISTRY C

Article

Quantum Master Equation Approach to Exciton Recurrence Motion in Ring-Shaped Aggregate Complexes Induced by Linear- and Circular-Polarized Laser Fields

Takuya Minami, Hitoshi Fukui, Hiroshi Nagai, Kyohei Yoneda,
Ryohei Kishi, Hideaki Takahashi, and Masayoshi Nakano

J. Phys. Chem. C, **2009**, 113 (8), 3332-3338• DOI: 10.1021/jp8096555 • Publication Date (Web): 03 February 2009

Quantum Master Equation Approach to Exciton Recurrence Motion in Ring-Shaped Aggregate Complexes Induced by Linear- and Circular-Polarized Laser Fields

Takuya Minami, Hitoshi Fukui, Hiroshi Nagai, Kyohei Yoneda, Ryohei Kishi, Hideaki Takahashi, and Masayoshi Nakano*

Department of Materials Engineering Science, Graduate School of Engineering Science, Osaka University, Toyonaka, Osaka 560-8531, Japan

Received: November 1, 2008; Revised Manuscript Received: December 18, 2008

The coherent exciton dynamics in molecular complexes composed of ring-shaped aggregates induced by linear- and circular-polarized laser fields has been investigated by using the quantum master equation (QME) approach. As shown in previous studies, near-degenerate states create the superposition states after irradiation of linear-polarized laser fields and thus cause the oscillatory exciton recurrence motion. In contrast, the rotatory exciton recurrence motion is found to be induced by circular-polarized laser field in a C_3-symmetry complex composed of identical three ring-shaped aggregates. This exciton dynamics is predicted to originate in the superposition states between the two pairs of degenerate states, which are coherently excited by a circular-polarized laser field. The rotatory exciton recurrence motion induced by a two-mode laser field with mutually opposite circular polarizations also has been examined in the complex composed of two different-sized groups of ring-shaped aggregates. It turns out that the two-mode laser field induces mutually counter-rotatory exciton recurrence motions concurrently, which are generated separately on the two different groups of ring-shaped aggregates. These results suggest the possibility of controlling rotatory exciton recurrence motions by using the circular-polarized laser fields and ring-shaped aggregate complexes.

1. Introduction

The coherent dynamics of exciton (electron−hole pair) or electron in molecules and molecular aggregates has been intensively investigated toward a fundamental understanding of dynamics of excited states and a new development of molecular-based nanoscale devices.[1−24] As is well-known, coherent excitation by irradiating laser fields creates superposition states composed of plural excited states, causing the spatial oscillation of excitation, i.e., exciton recurrence motion,[25−32] among constituent monomers in aggregate systems. Recently, the exciton recurrence motion between two identical chromophores [2,2′-binaphthyl (BN)] in solution has been experimentally observed by probing the fluorescence anisotropy decay by Hochstrasser and co-workers.[26] Yamazaki et al. have observed the oscillatory anisotropy decay for anthracene dimer, i.e., dithiaanthracenophane (DTA) in solution, which is longer than that for BN.[27] They have suggested the rigid and fixed molecular structure plays an important role in reducing the dephasing rate. On the other hand, there have been lots of studies on the coherent processes of intramolecular electron transfer. Using a quantum model simulation, Barth and Manz et al. have shown the periodic electron circulation in magnesium−porphyrin with cyclic structure, composed of four pyrroline subunits, induced by circular-polarized laser pulse.[33,34] They have predicted that the chirality of circular-polarized laser pulses can be transferred to unidirectional electron circulation on magnesium−porphyrin.

In our previous paper, we have theoretically investigated the exciton recurrence motion in several molecular aggregate models, i.e., dimer, trimer, and pentamer, composed of two-state monomers, under the classical and quantized laser fields.[30] We have found that the spatial behavior of exciton recurrence motion strongly depends on the aggregate structures, and have elucidated a novel generation mechanism of exciton recurrence motion in the quiescent region under quantized laser fields. On the other hand, the exciton recurrence motion induced by a circular-polarized laser field has not been investigated though it is highly expected to develop a novel control scheme of coherent exciton dynamics. In this study, we investigate the exciton recurrence motion induced by linear- and circular-polarized laser fields in C_2- and C_3-symmetry complexes composed of ring-shaped aggregates. The exciton dynamics in several molecular aggregate models after irradiation of linear- and circular-polarized laser fields are examined by the quantum master equation (QME) approach.[35,36] The nonrelaxation case is considered here because we focus on the elucidation of difference in the dynamical behavior purely induced by linear- and circular-polarized laser fields though the consideration of relaxation effects is important for experimental observations of recurrence motions in real systems.[31,32] We also examine the exciton recurrence motion in the complex of different-sized ring-shaped aggregates after irradiating a two-mode circular-polarized laser field, and discuss the possibility of controlling the rotatory exciton recurrence motion. These results will contribute to a novel development of creation and control schemes of oscillatory and rotatory exciton recurrence motions in supramolecular systems.

2. Methodology

The QME approach to the exciton dynamics in dipole−dipole coupled aggregate systems[31,32,35,36] is briefly explained in this section. This is performed in a manner of two-step procedures: (1) an exciton state model for an aggregate is constructed, and (2) the time-evolution of exciton is carried out by numerically solving the QME. We focus on the coherent process, i.e., exciton

* Corresponding author. Fax: +81 668506268. E-mail: mnaka@cheng.es.osaka-u.ac.jp.

10.1021/jp8096555 CCC: $40.75
Published on Web 02/03/2009

recurrence motion, in the one-exciton model, in which a pair of electron and hole is created in the aggregate. We consider a molecular aggregate model composed of two-state monomers with excitation energies $\{\omega_i\}$ and the magnitudes of transition moments $\{\mu_i\}$ ($i = 1, 2,..., N$; where N is the number of monomers). The present aggregate model can describe the exciton dynamics in aggregates composed of monomers, in which one excited state (per monomer) is resonated by a relatively weak laser field so as not to induce multiexciton processes. The Hamiltonian H_s for the molecular aggregate is expressed by

$$H_s = \sum_i^N \omega_i |i\rangle\langle i| + \frac{1}{2}\sum_{i,j}^N J_{ij}|i\rangle\langle j| \quad (1)$$

Here, $|i\rangle$ indicates the aggregate basis, which represents the situation that monomer i is excited, and J_{ij} represents the dipole−dipole coupling constant between monomers i and j with an intermolecular distance R_{ij}, which is given by

$$J_{ij} = \frac{1}{R_{ij}^3}\mu_i\mu_j\{\cos(\theta_{ij} - \theta_{ji}) - 3\cos\theta_{ij}\cos\theta_{ji}\} \quad (2)$$

$\theta_{ij}(\theta_{ji})$ is the angle between the transition moment of monomer $i(j)$ and the vector drawn from monomer i to j. The one-exciton states $\{|\psi_\alpha\rangle\}$ with excitation energies $\{\omega_\alpha\}$ and transition moments ($\mu_{\alpha,\beta} = \mu^x_{\alpha,\beta}\boldsymbol{e}_x + \mu^z_{\alpha,\beta}\boldsymbol{e}_z$, where $\boldsymbol{e}_x$ and $\boldsymbol{e}_z$ represent the unit vectors orthogonally oriented to each other on the aggregate plane, i.e., $z-x$ plane) obtained by a diagonalization of H_s matrix are expressed as

$$|\psi_\alpha\rangle = \sum_i^N |i\rangle\langle i|\psi_\alpha\rangle \equiv \sum_i^N C_{i\alpha}|i\rangle \quad (\alpha = 2, ..., M) \quad (3)$$

where M is equal to $N + 1$ in the one-exciton model, and $\alpha = 1$ indicates the vacuum state of exciton.

In this study, we consider the application of external continuous wave (cw) laser field with linear- or circular-polarization to the aggregate systems in order to create one-exciton. The linear-polarized laser field is represented by

$$\boldsymbol{F} = F\boldsymbol{e}_x\cos\omega t \quad (4)$$

where F and ω represent the amplitude and frequency of applied laser field, respectively. On the other hand, left (+)/right (−)-hand circular-polarized laser field is expressed as

$$\boldsymbol{F} = F(\boldsymbol{e}_x\cos\omega t \pm \boldsymbol{e}_z\sin\omega t) \quad (5)$$

where the left- and right-hand circular-polarization are defined as the *clockwise* and *anticlockwise* rotations of polarizations, respectively, when viewed along the direction of the field propagation.

The time-evolution of the on- and off-diagonal exciton density matrices in the exciton state basis $\{|\psi_\alpha\rangle\}$ is performed by using the QME in the Born−Markov approximation:[35,36]

$$\frac{d\rho_{\alpha\alpha}}{dt} = -\sum_m^M \Gamma_{\alpha\alpha;mm}\rho_{mm} + i\boldsymbol{F}\sum_n^M(\mu_{\alpha n}\rho_{n\alpha} - \rho_{\alpha n}\mu_{n\alpha}) \quad (6)$$

and

$$\frac{d\rho_{\alpha\beta}}{dt} = -i(\omega_\alpha - \omega_\beta)\rho_{\alpha\beta} - \sum_{m,n}^M \Gamma_{\alpha\beta;mn}\rho_{mn} + i\boldsymbol{F}\sum_n^M(\mu_{\alpha n}\rho_{n\beta} - \rho_{\alpha n}\mu_{n\beta}) \quad (\alpha \neq \beta) \quad (7)$$

Equations 6 and 7 are numerically solved by the fourth-order Runge−Kutta method. The spatial dynamics of exciton distribution is obtained by the basis conversion from the delocalized exciton state basis $\{|\psi_\alpha\rangle\}$ to the localized aggregate basis $\{|i\rangle\}$:

$$\rho_{ii}(t) = \sum_{\alpha,\beta}^M \langle i|\psi_\alpha\rangle\langle\psi_\alpha|\rho(t)|\psi_\beta\rangle\langle\psi_\beta|i\rangle = \sum_{\alpha,\beta}^M C_{i\alpha}\rho_{\alpha\beta}(t)C^*_{i\beta} \quad (8)$$

Using eqs 6, 7, and 8, the spatial exciton dynamics after cutting off the applied laser field at t_0 is described by

$$\rho_{ii}(t) = \sum_\alpha^M\sum_m^M C^*_{i\alpha}C_{i\alpha}\rho_{\alpha\alpha}(t_0)e^{-\Gamma_{\alpha\alpha;mm}t} + 2\sum_{\alpha>\beta}^M\sum_{m,n}^M C^*_{i\alpha}C_{i\beta}e^{-\Gamma_{\alpha\beta;mn}t}|\rho_{\alpha\beta}(t_0)| \times \cos\left[(\omega_\alpha - \omega_\beta)t - \arctan\left(\frac{\mathrm{Im}[\rho_{\alpha\beta}(t_0)]}{\mathrm{Re}[\rho_{\alpha\beta}(t_0)]}\right)\right] \quad (9)$$

We here consider the nonrelaxation case ($\Gamma_{\alpha\alpha;mm} = \Gamma_{\alpha\beta;mn} = 0$) in order to highlight the effects of the exciton-field interaction on the exciton recurrence motion. If there is only one superposition state and the product of the expansion coefficients on monomers i and j satisfies the following condition,

$$C_{i\alpha}C_{i\beta} > 0 \quad \text{and} \quad C_{j\alpha}C_{j\beta} < 0 \quad (10)$$

the exciton population on monomers i and j exhibits an opposite phase oscillation, i.e., oscillatory exciton recurrence motion between monomers i and j. On the other hand, if there are plural superposition states with mutually different energy differences ($\omega_\alpha - \omega_\beta$) and oscillation phases arctan(Im[$\rho_{\alpha\beta}$]/Re[$\rho_{\alpha\beta}$]), the linear combinations of $\rho_{\alpha\beta}$, modulated by $C_{i\alpha}C_{i\beta}$, are predicted to cause various phase shifts in ρ_{ii}. It is expected for plural superposition states that a circular-polarized field has the possibility of causing rotatory exciton recurrence motions as a series of these oscillations in ρ_{ii} with various phase shifts if appropriate aggregate structures are chosen.

3. Ring-Shaped Aggregate [Model a]

Figure 1a shows the ring-shaped aggregate composed of eight two-state monomers (shown by thick arrows) with an excitation energy of 38 000 cm^{-1} and the magnitude of a transition moment of 10 D, which are employed in our previous studies.[32,35] It is here noted that the choice of these quantities does not affect the essential results in this study though the change in the energy splitting of exciton states (caused by the different dipole−dipole interaction) varies the frequency of exciton recurrence motion (see eq 9). The adjacent intermonomer distance is fixed to be 15 au The one-exciton states of the aggregate system are obtained by diagonalizing the Hamiltonian H_s (eq 1). Figure 2a shows the multistep exciton states together with excitation energies and the magnitudes of transition moments. The magnitudes of transition moments are calculated by $\mu_{1\alpha} = [(\mu^x_{1\alpha})^2 + (\mu^z_{1\alpha})^2]^{1/2}$. Exciton states 3 and 4 are degenerate because of the two-dimensional aggregate structure with rotational symmetry. Figure 3a plots the expansion coefficients of exciton states 3 and 4, the size of the circle represents the magnitude of the expansion coefficient, and the black and white circles represent negative and positive phases of coefficients, respectively. Considering the rotational symmetry of monomer configuration (Figure 1a), such large transition moment amplitudes are realized since the exciton state has only one node line and the transition moment lies in a parallel direction to the node line (see Figure 3a). Other exciton states are not generated by the incident laser field since the transition moments are canceled by each other. Because the superposition state involving exciton

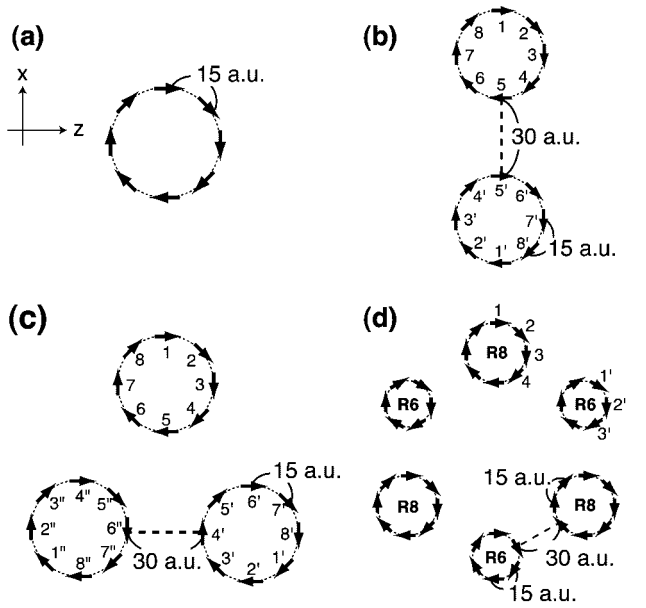

Figure 1. Structures of ring-shaped aggregate (a), C_2-symmetry complex of ring-shaped aggregates (b), C_3-symmetry complex of ring-shaped aggregates (c), and complex composed of **R6** and **R8** (d), which are the ring-shaped aggregates composed of six and eight monomers, respectively, with identical two-state models (excitation energy ω_i = 38 000 cm^{-1} and transition moment μ_i = 10 D). The adjacent intermonomer distance in a ring and the adjacent interring distance are 15 and 30 au, respectively.

states with energy differences is indispensable for generating the exciton recurrence motion as shown in eq 9, model a does not show the exciton recurrence motion even if degenerate states 3 and 4 are coherently excited by irradiation of a laser field.

4. C_2-Symmetry Complex of Two Ring-Shaped Aggregates [Model b]

Figure 1b shows the structure of the C_2-symmetry complex of two ring-shaped aggregates. The adjacent intermonomer and interring distances are fixed to be 15 and 30 au, respectively. Inserted monomer numbers are numbered in clockwise order as satisfying C_2-symmetry. The excitation energies and the transition moments are shown in Figure 2b. There is a pair of near-degenerate states, 4 and 6, with large transition moment amplitudes, the slight energy difference of which is derived from the energy splitting of the exciton states of ring-shaped aggregate a (Figure 2a) caused by the small J- and H-aggregate type interring interactions in the C_2-symmetry (linear) structure of model b. Figure 3b plots the expansion coefficients in exciton states 4 and 6. Similarly to model a, each ring-shaped aggregate in exciton states 4 and 6 exhibits a large transition moment amplitude since the exciton state has a node line, while the other exciton states exhibit no transition moments due to the cancelation among transition moments in the constituent rings.

Figure 4 shows the exciton dynamics (using eqs 6 and 7) in model b induced by three kinds of laser fields, i.e., the left-hand circular-polarized laser field (L), right-hand circular-polarized laser field (R), and linear-polarized laser field (P). The frequency of 36 650 cm^{-1} is chosen to be in near-resonance with both exciton states 4 and 6, and the field power and irradiating cycles are fixed to be 10 MW/cm^2 and 1000 optical cycles (~0.91 ps), respectively. The inserted pictures show the exciton distributions at the corresponding times (shown by vertical dotted lines). The oscillatory exciton dynamics appears in model b after irradiation of the circular-polarized laser field

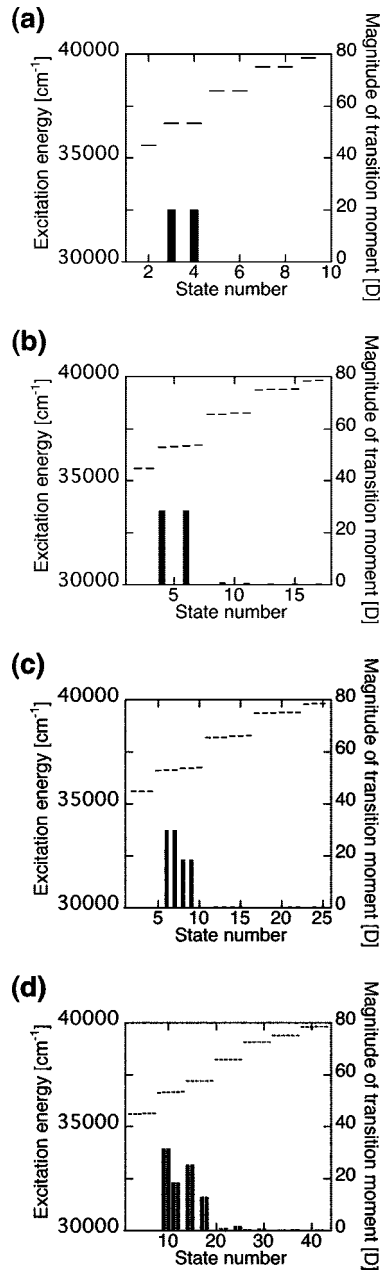

State	ω_α [cm^{-1}]	$\mu^x_{1\alpha}$ [D]	$\mu^z_{1\alpha}$ [D]
3	36667	-0.63	-19.99
4	36667	19.99	-0.63

State	ω_α [cm^{-1}]	$\mu^x_{1\alpha}$ [D]	$\mu^z_{1\alpha}$ [D]
4	36618	-28.28	0.00
6	36690	0.00	-28.28

State	ω_α [cm^{-1}]	$\mu^x_{1\alpha}$ [D]	$\mu^z_{1\alpha}$ [D]
6	36618	-23.54	17.78
7	36618	-17.78	-23.54
8	36701	-13.20	-12.46
9	36701	12.46	-13.20

State	ω_α [cm^{-1}]	$\mu^x_{1\alpha}$ [D]	$\mu^z_{1\alpha}$ [D]
9	36654	22.72	-21.43
10	36654	-21.43	-22.72
11	36671	-12.80	-12.89
12	36671	-12.89	12.80
14	37192	19.77	15.42
15	37192	15.42	-19.77
17	37207	-1.09	-12.73
18	37207	12.73	-1.09

Figure 2. Excitation energies, ω_α, and the magnitude of the transition moments (shown by bar graphs), $\boldsymbol{\mu}_{1\alpha}$, between the ground (1) and exciton states (α) for models a, b, c, and d. Numerical values of the excitation energies (ω_α) and the x- and z-components of transition moments ($\mu^x_{1\alpha}$, $\mu^z_{1\alpha}$) are also shown.

(see Figure 4L,R), whereas the stationary exciton population is observed after irradiation of the linear-polarized laser field (see Figure 4P). The absence of the oscillatory behavior of exciton population in the linear-polarized laser field originates in the absence of the transition moment between the ground and exciton state 6 in the x-direction, which is parallel to the polarization of the linear-polarized laser field (see state 6 in Figure 2b). As shown in Figure 4L,R, the oscillatory recurrence motion of exciton is observed between monomers (2, 2′, 6, 6′) shown by blue triangles and (4, 4′, 8, 8′) shown by black inverted triangles, while the stationary exciton population is observed in monomers (1, 1′, 5, 5′) shown by red circles and (3, 3′, 7, 7′) shown by green squares, the feature of which is derived from the absence of the overlap of the exciton distribution, $C_{i\alpha}C_{i\beta}$ on monomer i = (1, 1′, 5, 5′, 3, 3′, 7, 7′) between exciton states 4 and 6 (see Figure 3b and eq 9). It is

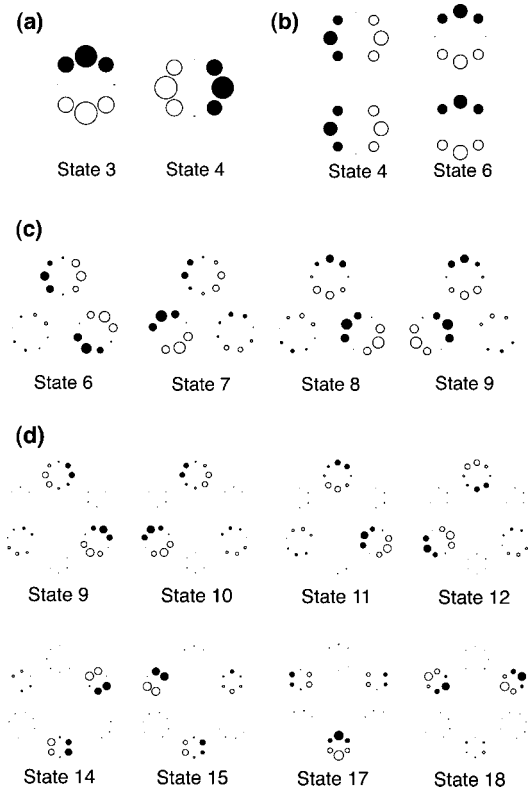

Figure 3. Spatial configurations of expansion coefficients with large transition moments of models a, b, c, and d. The white and black circles indicate the positive and negative expansion coefficients, respectively, and the size of the circle represents the magnitude of the expansion coefficient.

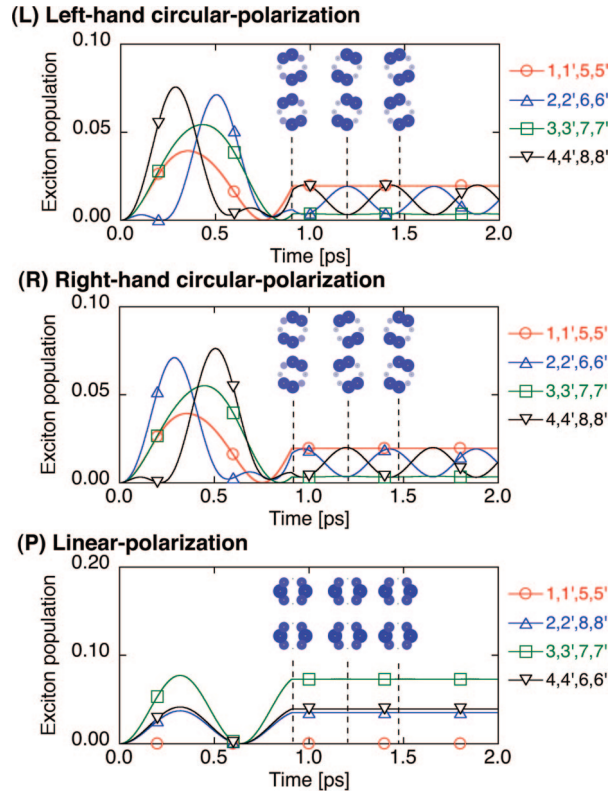

Figure 4. Time evolution of exciton populations in the aggregate basis for model b after irradiating three types of laser fields for 1000 optical cycles with left-hand circular-polarization (L), right-hand circular polarization (R), and linear (plane)-polarization (P). The field power and the frequency are 10 MW/cm^2 and 36 650 cm^{-1}, respectively.

noted that the oscillatory phases of exciton population between monomers (2, 2′, 6, 6′) and (4, 4′, 8, 8′) are opposite between parts L and R in Figure 4 (see blue and black curves) because the oscillation of off-diagonal density matrix $\rho_{4,6}$, which occurs between monomers (2, 2′, 6, 6′) and (4, 4′, 8, 8′), exhibits the mutually opposite phase oscillation between the left- and right-hand circular-polarized laser fields due to their mutually opposite oscillatory phases of z-polarizations (see eq 5). These results substantiate that the polarization of the circular-polarized laser field affects the oscillatory phases of off-diagonal density matrices, and thus cause the phase shift in exciton recurrence motion.

5. C_3-Symmetry Complex of Three Ring-Shaped Aggregates [Model c]

Figure 1c shows the structure of the C_3-symmetry complex of three ring-shaped aggregates. The adjacent intermonomer and interring distances are fixed to be 15 and 30 au, respectively. The excitation energies and the transition moments are shown in Figure 2c. It is noted that there are two pairs of degenerate states, (6, 7) and (8, 9), with large transition moment amplitudes originating in the two-dimensional C_3-symmetry structure, in contrast to the near-degenerate exciton states of model b originating in the one-dimensional C_2-symmtery structure (see Figure 2b). It is generally predicted that the complexes of ring-shaped aggregates with n-fold ($n \geq 3$) rotational symmetry provide plural pairs of degenerate states with large transition moment amplitudes because of the two-dimensional rotational symmetry as well as the J- or H-aggregate type interring interactions. For model c, the superposition states between the two pairs of degenerate states, (6, 7) and (8, 9) (see Figure 3c for plots of the expansion coefficients), turn out to cause the four oscillatory off-diagonal density matrices ($\rho_{6,8}$, $\rho_{6,9}$, $\rho_{7,8}$, $\rho_{7,9}$) with the same frequency, which is derived from the energy difference between the two pairs of degenerate states (see eq 9 and Figure 2c).

Figure 5 shows the exciton dynamics (using eqs 6 and 7) of the C_3-symmetry complex of three ring-shaped aggregates induced by three kinds of laser fields, i.e., the left-hand circular-polarized laser field (L), right-hand circular-polarized laser field (R), and the linear-polarized laser field (P). The frequency of 36 650 cm^{-1} is chosen to be in near-resonance with exciton states, (6, 7) and (8, 9), and the power and the irradiating cycles are fixed to be 10 MW/cm^2 and 1000 optical cycles (∼0.91 ps), respectively. The exciton distributions at times t_i (i = 1, 2,...) are also shown in Figure 5. As seen in parts L and R of Figure 5, the four kinds of oscillation phases of exciton populations, (1, 1′, 1″, 5, 5′, 5″) shown by red circles, (2, 2′, 2″, 6, 6′, 6″) shown by blue-filled triangles, (3, 3′, 3″, 7, 7′, 7″) shown by green squares, and (4, 4′, 4″, 8, 8′, 8″) shown by black-filled inverted triangles, are induced by the circular-polarized laser field, while only two kinds of oscillation phases of exciton populations, (1′, 1″, 5′, 5″, 4′, 8′, 2″, 6″) shown by solid lines and (1, 5, 2, 8, 3, 7, 4, 6, 2′, 6′, 4″, 8″, 3′, 7′, 3″, 7″) shown by dotted lines, are induced by the linear-polarized laser field (see Figure 5P). The circular-polarized laser field interacting with both x- and z-components of transition moments exhibits mutually orthogonal oscillation phases (see eq 5). In addition, a pair of degenerate states has the transition moments in mutually orthogonal direction (see $\mu^x_{1\alpha}$ and $\mu^z_{1\alpha}$ in Figure 2c). It is thus predicted that a pair of degenerate states is excited with mutually orthogonal phases by the circular-polarized laser field, and then the coherent excitation of the two pairs of

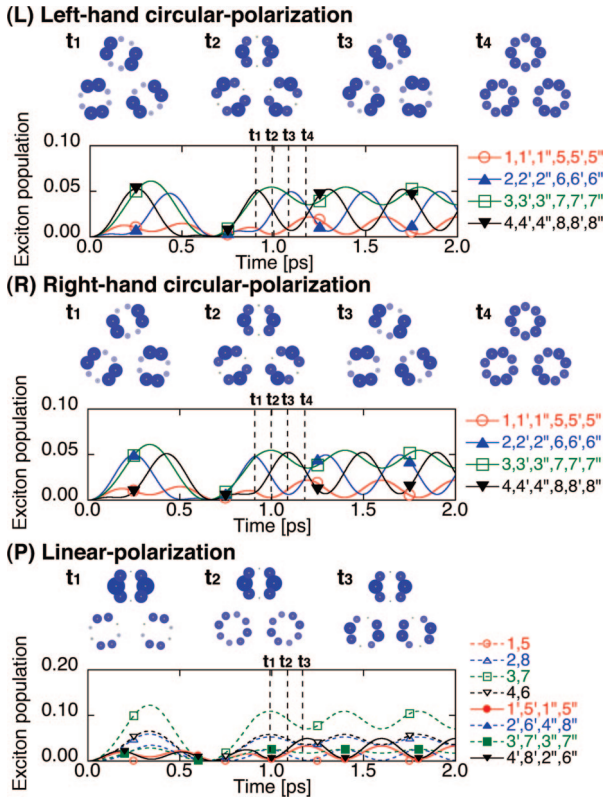

Figure 5. Time evolution of exciton populations in the aggregate basis for model c after irradiating three types of laser fields for 1000 optical cycles. See Figure 4 for further legends.

degenerate states causes several out-of-phase oscillations in the off-diagonal density matrices $\{\rho_{\alpha\beta}\}$. Therefore, out-of-phase oscillations of exciton populations (ρ_{ii}) are generated on monomers $\{i\}$ due to the linear combination of the four kinds of off-diagonal density matrices $\{\rho_{\alpha\beta}\}$ with the same frequency and different oscillation phases. It is noted that the realization of this feature requires the coherent excitation of two pairs of degenerate states by the circular-polarized laser field. On the other hand, in the linear-polarized laser field, the absence of mutually orthogonal oscillation phases in polarization leads to only the mutually opposite phase oscillations of exciton populations (ρ_{ii}) on monomers $\{i\}$ because of the linear combination of off-diagonal density matrices with the same or mutually opposite oscillatory phase depending on the sign of the product of expansion coefficients, $C_{i\alpha}C_{i\beta}$ (see eqs 9 and 10).

It is found that the exciton population in the case of left-hand circular polarization takes extrema in order of (4, 4′, 4″, 8, 8′, 8″), (3, 3′, 3″, 7, 7′, 7″), (2, 2′, 2″, 6, 6′, 6″), and (1, 1′, 1″, 5, 5′, 5″), corresponding to the *anticlockwise* rotation of exciton population (see Figure 5L), while the exciton population in the case of right-hand circular polarization takes extrema in order of (1, 1′, 1″, 5, 5′, 5″), (2, 2′, 2″, 6, 6′, 6″), (3, 3′, 3″, 7, 7′, 7″), and (4, 4′, 4″, 8, 8′, 8″), corresponding to the *clockwise* rotation of exciton population (see Figure 5R). Namely, the rotational direction of exciton is opposite to that of the polarization of the incident laser field. The exciton distributions shown in parts L and R of Figure 5 sustain the C_3-symmetry exciton distribution at each time. This indicates that the symmetry of the aggregate structure affects the dynamics of rotatory recurrence motion of exciton in the circular-polarized laser field case. In contrast, it turns out that the linear-polarized laser field does not induce the rotatory recurrence motion of exciton, while alternatively inducing the oscillatory recurrence motion originating in the mutually opposite phase oscillation of exciton population (see Figure 5P).

On the basis of the above results, it turns out that in the C_3-symmetry complex composed of ring-shaped aggregates, the rotatory recurrence motion of exciton is generated when two pairs of degenerate states are coherently excited by a circular-polarized laser field.

6. Complex of Different-Sized Ring-Shaped Aggregates [Model d]

6.1. Structure and Exciton States. Figure 1d shows the structure of the complex composed of two kinds of ring-shaped aggregates **R6** and **R8**, which are the ring-shaped aggregates composed of six and eight monomers, respectively, with an adjacent intermonomer distance of 15 au. Both **R6**- and **R8**-groups have C_3-symmetry structures, and the adjacent **R6**−**R8** distance is fixed to be 30 au. Figure 2d shows the excitation energies and transition moments. There are four pairs of degenerate states with a relatively large energy difference of about 540 cm^{-1} between exciton states (9, 10, 11, 12) and (14, 15, 17, 18) in contrast to the small energy differences of 17.0 cm^{-1} between exciton states (9, 10) and (11, 12), and 14.6 cm^{-1} between exciton states (14, 15) and (17, 18). Figure 3d plots the expansion coefficients of the exciton states with large transition moments. Localized exciton distributions in **R6**- and **R8**-groups are observed in exciton states (14, 15, 17, 18) and (9, 10, 11, 12), respectively, the feature of which originates in the large energy difference between those exciton states of **R6** and **R8**. It is expected that an appropriately tuned single mode laser field separately excites the **R6**- and **R8**-groups because of the relatively large energy difference and spatially well-separated exciton distributions between exciton states (9, 10, 11, 12) and (14, 15, 17, 18). The two well-separated exciton distributions are also expected to cause a slight interference between exciton states (9, 10, 11, 12) and (14, 15, 17, 18), originating in the slight overlap ($C_{i\alpha}C_{i\beta}$) between the exciton distributions (see Figure 3d and eq 9).

6.2. Exciton Dynamics Induced by a Single Mode Laser Field. The exciton population dynamics in model d induced by a single mode laser field with a left-hand circular-polarization is performed by using eqs 6 and 7. The power and the irradiating cycles of the incident laser field are fixed to be 10 MW/cm^2 and 1000 optical cycles ($t_1 \approx 0.9$ ps), respectively. The frequency is chosen to be either 37 200 cm^{-1} (I) in near-resonance with states (14, 15, 17, 18) or 36 660 cm^{-1} (II) in near-resonance with states (9, 10, 11, 12). Figure 6 shows the exciton population dynamics on monomers (1, 2, 3, 4) belonging to the **R8**-group (shown by unfilled marks) and (1′, 2′, 3′) belonging to the **R6**-group (shown by filled marks). As shown in the dynamics after cutting field at t_1 (see Figure 6I), the exciton recurrence motion is observed in the **R6**-group, whereas the exciton is not generated in the **R8**-group in the case of irradiation with a frequency of 37 200 cm^{-1}. The exciton population takes extrema in order of 3′, 2′, and 1′, which corresponds to the synchronous *anticlockwise* rotation of exciton population on each ring belonging to the **R6**-group. On the other hand, as shown in Figure 6II, the exciton recurrence motion is induced only in the **R8**-group in the case of irradiation with a frequency of 36 660 cm^{-1}. The exciton population takes extrema in order of 4, 3, 2, and 1, which also corresponds to the synchronous *anticlockwise* rotation of exciton on each ring belonging to the **R8**-group. These spatially separated exciton generations originate in the large energy difference between exciton states (9, 10, 11, 12) and (14, 15, 17, 18) as well as the

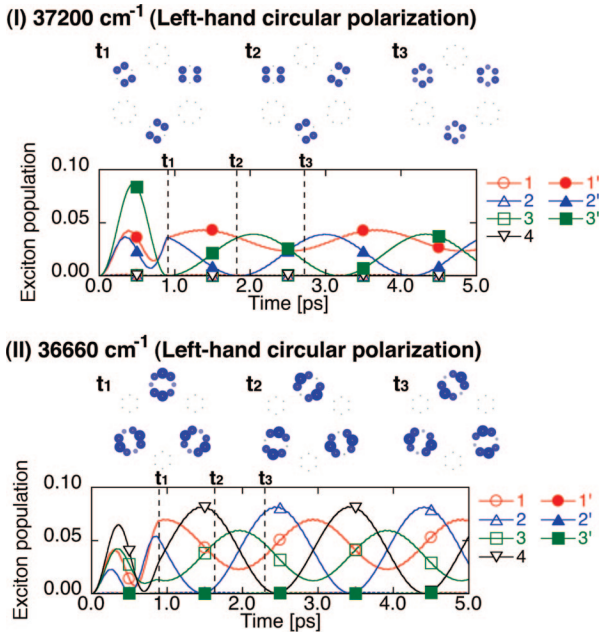

Figure 6. Time evolution of exciton populations in the aggregate basis for model d after irradiating two types of single-mode left-hand circular-polarized laser fields for 1000 optical cycles. The field power is 10 MW/cm^2, and the frequencies of two types of fields are 37 200 cm^{-1} (I), which is near-resonant with the **R6**-group, and 36 660 cm^{-1} (II), which is near-resonant with the **R8**-groups, respectively.

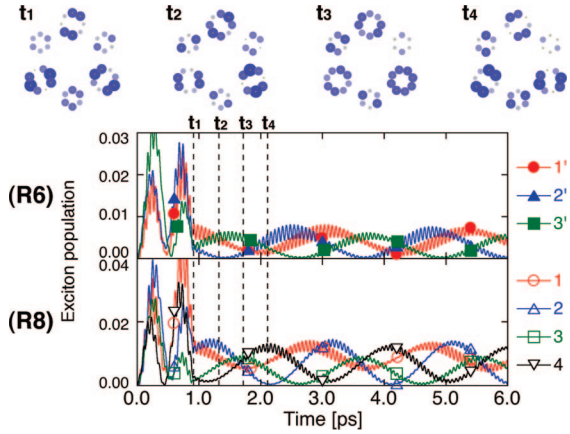

Figure 7. Time evolution of exciton populations in the aggregate basis for model d after irradiating a two-mode laser field with a power of 10 MW/cm^2 for 1000 optical cycles: the first mode field has a left-hand circular-polarization with a frequency of 37 200 cm^{-1}, and the second has a right-hand circular-polarization with a frequency of 36 660 cm^{-1}.

spatially well-separated exciton distributions between these groups of exciton states. In addition, similarly to model c, the rotatory exciton recurrence motion is predicted to originate in the C_3-symmetry structure of **R6**- or **R8**-groups and the circular-polarized laser field. These results indicate that an appropriately tuned single mode circular-polarized laser field can selectively excite the **R6**- and **R8**-groups in this type of complex, inducing the rotatory recurrence motion of exciton in the opposite direction as the rotational direction of the polarization vector of the incident laser field.

6.3. Exciton Dynamics Induced by a Two-Mode Laser Field. Figure 7 shows the exciton dynamics in model d induced by a two-mode laser field with mutually opposite circular polarizations. The frequencies of the incident laser field are respectively chosen to be in near-resonance with the exciton states corresponding to two aggregate groups **R8** and **R6**: the first laser field has the frequency of 37 200 cm^{-1} [in near-resonance with exciton states (14, 15, 17, 18) with localized distribution in the **R6**-group] and left-hand circular-polarization, while the second one has the frequency of 36 660 cm^{-1} [in near-resonance with exciton states (9, 10, 11, 12) with localized exciton distribution in the **R8**-group] and right-hand circular-polarization (see Figures 2d and 3d). The exciton dynamics on **R6**- and **R8**-groups is shown in Figure 7. The mutually counter-rotatory motions, though they also carry rapid oscillations with smaller amplitudes, are primarily observed well-separated on **R6**- and **R8**-groups, which exhibit the synchronous *anticlockwise* and *clockwise* exciton rotations in each ring, respectively. These mutual counter-rotations reflect the relation between the rotation directions of two polarization vectors of the two-mode near-resonance circular-polarized laser field. The carried rapid oscillations, which are also slightly seen in the single-mode laser field case (see Figure 6), are caused by the interference between exciton states (9, 10, 11, 12) and (14, 15, 17, 18), slight fractions of which are superposed by the two-mode laser field. Indeed, the rapid oscillation frequency roughly corresponds to the energy difference between these exciton states.

It is concluded that an appropriate two-mode laser field can simultaneously control the exciton recurrence motions with different rotational directions under the following conditions: (1) well-separated exciton distribution between different pairs of the degenerate states and (2) selective generation of exciton states corresponding to different aggregate groups. In the present model [model d], these conditions are achieved by the two different-sized ring-shaped aggregates (**R6**- and **R8**-aggregate groups) and a two-mode laser field with left/right-circular polarizations and different frequencies, which are near-resonant with the two kinds of exciton states corresponding to **R6**- and **R8**-groups, respectively.

7. Summary

We have investigated the exciton recurrence motion in ring-shaped aggregate complex models b, c, and d using the QME approach. It is clarified that the realization of rotatory recurrence motion of exciton requires the irradiation of circular-polarized laser field and, at least, two pairs of degenerate exciton states with mutually orthogonal transition moments, the conditions of which are satisfied by the rotational symmetry configuration of monomers in a ring-shaped aggregate and its complex. It is thus predicted that the realization of rotatory recurrence behavior is independent from the number of monomers n (though $n > 4$ is needed for determining the rotation direction) in a ring-shaped aggregate or the order of rotational symmetry for the ring complexes, as long as there are plural pairs of degenerate states contributing to superposition states. In addition, the rotational direction of exciton turns out to be opposite to the rotational direction of incident circular-polarized laser field in the present models. We also have predicted the simultaneous induction of mutually opposite rotatory recurrence motion of exciton in an aggregate complex using a two-mode near-resonant laser field with mutually opposite circular polarizations if the system possesses two kinds of ring-shaped aggregate groups, which give two groups of exciton states (with a large energy interval) and thus have mutually well-separated exciton distributions. The present exciton recurrence motions are expected to be exemplified by analyzing the oscillatory and/or rotatory pattern of polarized fluorescence intensity similarly to the previous experimental study.[27]

Although the present study has been performed without relaxation effects because we focus on the mechanism of the rotatory exciton recurrence motion and the relation to the aggregate structure, the consideration of relaxation effects on exciton recurrence motion is indispensable for experimental observation in real systems, and is also intriguing from the viewpoint of the fundamental understanding of decoherence processes. Such points will be addressed at the next stage as well as further quest for other intriguing exciton recurrence dynamics.

Acknowledgment. This work is supported by Grant-in-Aid for Scientific Research (Nos. 18350007 and 20655003) from the Japan Society for the Promotion of Science (JSPS), Grant-in-Aid for Scientific Research on Priority Areas (No. 18066010) from the Ministry of Education, Science, Sports and Culture of Japan, and the global COE (center of excellence) program "Global Education and Research Center for Bio-Environmental Chemistry" of Osaka University.

Supporting Information Available: Movies of exciton dynamics corresponding to Figures 4, 5, 6, and 7. This material is available free of charge via the Internet at http://pubs.acs.org.

References and Notes

(1) Tretiak, S.; Mukamel, S. *Chem. Rev.* **2002**, *102*, 3171.
(2) Mukamel, S.; Tretiak, S.; Wagersreiter, T.; Chernyak, V. *Science* **1997**, *277*, 781.
(3) Sension, R. J. *Nature* **2007**, *446*, 740.
(4) Ogawa, T.; Tokunaga, E.; Kobayashi, T. *Chem. Phys. Lett.* **2005**, *408*, 186.
(5) Mülken, O.; Bierbaum, V.; Blumen, A. *J. Chem. Phys.* **2006**, *124*, 124905.
(6) Varnavski, O. P.; Ostrowski, J. C.; Sukhomlinova, L.; Twieg, R. J.; Bazan, G. C.; Goodson, T., III *J. Am. Chem. Soc.* **2002**, *124*, 1736.
(7) Kenkre, V. M.; Schmid, D. *Phys. Rev. B* **1985**, *31*, 2430.
(8) Kumble, R.; Hochstrasser, R. M. *J. Chem. Phys.* **1998**, *109*, 855.
(9) van Grondelle, R.; Novoderezhkin, V. I. *Phys. Chem. Chem. Phys.* **2006**, *8*, 793.
(10) Kühn, O.; Sundholm, V.; Pullerits, T. *Chem. Phys.* **2002**, *275*, 15.
(11) Barvik, I.; Herman, P. *Phys. Rev. B* **1992**, *45*, 2772.
(12) Engel, G. S.; Calhoun, T. R.; Read, E. L.; Ahn, T.-K.; Mančal, T.; Cheng, Y.-C.; Blankenship, R. E.; Fleming, G. R. *Nature* **2007**, *446*, 782.
(13) Cheng, Y.-C.; Engel, G. S.; Fleming, G. R. *Chem. Phys.* **2007**, *341*, 285.
(14) Gaab, K. M.; Bardeen, C. J. *J. Chem. Phys.* **2004**, *121*, 7813.
(15) Ohta, K.; Yang, M.; Fleming, G. R. *J. Chem. Phys.* **2001**, *115*, 7609.
(16) Pisliakov, A. V.; Mančal, T.; Fleming, G. R. *J. Chem. Phys.* **2006**, *124*, 234505.
(17) Lee, H.; Cheng, Y.-C.; Fleming, G. R *Science* **2007**, *316*, 1462.
(18) Hyeon-Deuk, K.; Tanimura, Y.; Cho, M. *J. Chem. Phys.* **2008**, *128*, 135102.
(19) Krause, P.; Klamroth, T.; Saalfrank, P. *J. Chem. Phys.* **2005**, *123*, 074105.
(20) Barth, I.; Manz, J.; Serrano-Andrés, L. *Chem. Phys.* **2008**, *347*, 263.
(21) Nobusada, K.; Yabana, K. *Phys. Rev. A* **2007**, *75*, 032518.
(22) Matos-Abiague, A.; Berakdar, J. *Phys. Rev. Lett.* **2005**, *94*, 166801.
(23) Nakano, M.; Kishi, R.; Nakagawa, N.; Nitta, T.; Yamaguchi, K. *J. Phys. Chem. B* **2005**, *109*, 7631.
(24) Nakano, M.; Kishi, R.; Minami, T.; Fukui, H.; Nagai, H.; Yoneda, K.; Takahashi, H. *Chem. Phys. Lett.* **2008**, *460*, 370.
(25) Kim, Y. R.; Share, P.; Pereira, M.; Sarisky, M.; Hochstrasser, R. M. *J. Chem. Phys.* **1989**, *91*, 7557.
(26) Zhu, F.; Gali, C.; Hochstrasser, R. M. *J. Chem. Phys.* **1993**, *98*, 1042.
(27) Yamazaki, I.; Akimoto, S.; Yamazaki, T.; Sato, S.; Sakata, Y. *J. Phys. Chem. A* **2002**, *106*, 2122.
(28) Yamazaki, I.; Aratani, N.; Akimoto, S.; Yamazaki, T.; Osuka, A. *J. Am. Chem. Soc.* **2003**, *125*, 7192.
(29) Yamazaki, I.; Akimoto, S.; Aratani, N.; Osuka, A. *Bull. Chem. Soc. Jpn.* **2004**, *77*, 1959.
(30) Nakano, M.; Ohta, S.; Kishi, R.; Nate, M.; Takahashi, H.; Furukawa, S. *J. Chem. Phys.* **2006**, *125*, 234707.
(31) Nitta, H.; Shoji, M.; Takahata, M.; Nakano, M.; Yamaki, D.; Yamaguchi, K. *J. Photochem. Photobiol. A* **2006**, *178*, 264.
(32) Minami, T.; Nakano, M.; Fukui, H.; Nagai, H.; Kishi, R.; Takahashi, H. *J. Phys. Chem. C* **2008**, *112*, 16675.
(33) Barth, M.; Manz, J.; Shigeta, Y.; Yagi, K. *J. Am. Chem. Soc.* **2006**, *128*, 7043.
(34) Barth, M.; Manz, J. *Angew. Chem., Int. Ed.* **2006**, *45*, 2962.
(35) Takahata, M.; Nakano, M.; Fujita, H.; Yamaguchi, K. *Chem. Phys. Lett.* **2002**, *363*, 422.
(36) Takahata, M.; Nakano, M.; Yamaguchi, K. *J. Theor. Comput. Chem.* **2003**, *2*, 459.

JP8096555